Proceedings of the 21st ICSMGE, Vienna, Austria, 14 – 19 June 2026. Pistrol, Adam & Schweiger (eds.)
Published by: ÖGG, Austrian Society for Geomechanics, Salzburg, Austria, ISBN 978-3-9503898-4-5
https://doi.org/10.53243/ICSMGE2026-195

Arbitrary Lagrangian-Eulerian method to analyse the disturbed zone around controlled modulus columns

Thishani Amarathunga, D S Liyanapathirana, W H Peellage, P Hu & C J Leo
School of Engineering Design and Built Environment, Western Sydney University, Australia
T.Amarathunga@westernsydney.edu.au

ABSTRACT: Ground improvement has become an important research area in geotechnical engineering due to the scarcity of naturally suitable ground conditions for construction. Application of column inclusions is one of the most popular ground improvement methods used in practice to reduce the loads transferred to the existing ground with low bearing capacity. One such technology is Controlled Modulus Columns (CMC), and they have gained popularity for their efficiency and simplicity in installation. CMC are installed using a displacement auger that laterally displaces surrounding soil. In sandy soils, CMC creates a compacted region, while in soft soils, it leads to partial consolidation and a region with reduced permeability around CMC. This study focuses on sandy soils to investigate the disturbed zone, which exhibits increased stiffness and strength relative to undisturbed ground, enhancing its ability to transfer loads. Despite its practical significance, behaviour of disturbed zone during and after CMC installation remains poorly understood in literature. This paper presents a detailed numerical investigation into installation effects of CMC in sandy soils, focusing on the formation and characteristics of the disturbed zone. Due to the large soil deformations and highly nonlinear soil behaviour involved in the installation process, conventional small-strain finite element methods are inadequate. To address these challenges, the Arbitrary Lagrangian-Eulerian (ALE) technique available in ABAQUS/Explicit is employed, enabling realistic simulation of large soil deformations. The constitutive behaviour of sand is modelled using the SANISAND model. Simulation results provide insights into the evolution of load-displacement behaviour, radial stress distribution, radial displacement and void ratio changes around the column during installation and highlight the development of significant densification and increased confinement within the disturbed zone as penetration depth increases. These findings contribute to a better understanding of ground modification mechanisms and provide a foundation for more accurate performance prediction and design optimisation of CMC.

KEYWORDS: Arbitrary Lagrangian-Eulerian, controlled modulus columns, ground improvement, large soil deformation, disturbed zone.

1 INTRODUCTION

Ground improvement techniques are essential for the stability and performance of geotechnical structures. These techniques are generally classified into two main categories: i) improving the properties of the existing ground through consolidation-based techniques for saturated soils and compaction-based techniques for dry sand, and ii) reducing the loads transferred to the existing ground through the use of rigid inclusions. Although compaction based methods are cost-effective for improvement of sandy soils at shallow depths, ground improvement using rigid inclusions such as Controlled Modulus Columns (CMC), Deep Cement Mixed (DCM) columns and stone or granular columns are the most effective in practice when ground improvement is required for deeper layers of ground. These methods are used to minimise the loads transferred to the weak subsurface, and they are suitable for many challenging ground conditions to increase the bearing capacity, minimise settlement, and improve stability. (Alamgir et al., 1996; Chu et al., 2009; Varaksin et al., 2014; Han, 2015).

CMC have gained popularity due to the straightforward and efficient nature of their installation process. CMC are installed with a displacement auger that laterally displaces the surrounding soil. This process creates a disturbed zone around columns due to the compaction of the surrounding soil. The soil within the disturbed zone has increased stiffness and strength compared to the in-situ ground, resulting in a zone with increased load-bearing capacity of the CMC. However, the understanding of the disturbed zone effects has not received much attention in the literature. (Massé et al., 2011; Larisch et al., 2015; Suleiman et al., 2016).

Therefore, in this paper, the installation effects of CMC on the surrounding soil will be investigated in detail. Due to large soil deformations and highly nonlinear material behaviour associated with installation, the CMC installation process cannot be simulated with conventional finite element programs based on small-strain assumptions. Therefore, the Arbitrary Lagrangian-Eulerian (ALE) method available in ABAQUS/Explicit is used in this paper, accommodating large soil deformations and soil nonlinearity. This study investigates Ottawa F65 sandy soil (Ramirez et al., 2018) and utilises the SANISAND constitutive model to simulate the constitutive behaviour of soil. The changes in in-situ soil properties within the disturbed zone and the radial extent of the disturbed zone during column installation are investigated.

2 ALE METHOD

The Arbitrary Lagrangian-Eulerian (ALE) method is a powerful numerical technique that combines the strengths of both Lagrangian and Eulerian formulations to effectively model problems involving large deformations. In traditional Lagrangian analysis, the mesh moves with the material, which can lead to excessive mesh distortion. Conversely, Eulerian analysis allows material to flow through a fixed mesh but may not capture material interfaces well. The ALE method offers a hybrid solution by decoupling material and mesh movements, enabling the mesh to move independently of the material and thus mitigating mesh distortion. ((Hu & Randolph, 1998; Liyanapathirana et al., 2000; Liyanapathirana, 2009; Wang et al., 2015)

ABAQUS/Explicit has ALE capabilities that are widely applied in geotechnical simulations, such as pile and column installation. The adaptive meshing technique in ABAQUS combines the strengths of pure Lagrangian and pure Eulerian analysis. Adaptive meshing in ABAQUS/Explicit is intended to model large deformation problems. ALE adaptive meshing differs from the pure Eulerian analysis feature available in ABAQUS/Explicit. The pure Eulerian capability enables the use of multiple materials and voids within one element, making it suitable for analyses involving significant deformations, like in fluid dynamics problems. In contrast, ALE elements are always completely filled with a single material. While this approach restricts the material deformation in the model to that

of the elements themselves, it allows for more accurate definitions of material boundaries and facilitates more complex contact interactions (Dassault-Système, 2025).

In the ALE approach, each incremental step includes a Lagrangian phase and an Eulerian phase. The first step of explicit Lagrangian analysis causes a distorted mesh, which requires a newly improved mesh for the next step. In the second step, variables in the previous analysis are transferred into the new mesh while performing an Eulerian analysis. During each time increment of the analysis, a smoothing technique is used to improve the quality of the finite element mesh, and mesh sweeps are performed after each increment. Although the quality of the mesh is preserved during the analysis, the same topology is used throughout the analysis (Wang et al., 2015; Yang et al., 2020). The ALE method allows the material and finite element mesh movements to be separated to avoid mesh distortion; re-meshing is employed to provide a suitable mesh quality throughout the calculation process. Due to its ability to combine the benefits of both Lagrangian and Eulerian formulations, ALE provides a generalised and robust platform for large deformation simulations. It is particularly well-suited for geotechnical applications, such as pile or column installations, where large soil displacements and nonlinear behaviour are prevalent (Ekanayake et al., 2013; Wang et al., 2015; Konkol & Bałachowski, 2016; Liyanapathirana & Ekanayake, 2016; Bakroon et al., 2017; Hannachi et al., 2021; Wotzlaw et al., 2024).

3 SANISAND MODEL

The SANISAND model (Dafalias & Manzari, 2004) is a constitutive model developed within the critical state framework to simulate the mechanical behaviour of sandy soils under various loading conditions. The term SANISAND refers to a series of models under the "Simple ANIsotropic SAND" framework, which incorporates principles from critical state soil mechanics and bounding surface plasticity. It is particularly designed to generate stress-strain responses for both dense and loose sands, under monotonic and cyclic loading, as well as other complex stress paths.

Three novel aspects distinguish the SANISAND model by Dafalias & Manzari (2004) from earlier versions, such as that of Manzari & Dafalias (1997). First, the dilatancy formulation is governed by a fabric-dilatancy tensor, which captures macroscopic effects of evolving fabric during loading. Second, the model introduces a dependence of the plastic deviatoric strain rate direction on a modified Lode angle, enhancing the model's ability to simulate multiaxial stress states. Third, the model defines consistent relationships between parameters in triaxial and multiaxial conditions, improving its generalisation and calibration capabilities (Manzari & Dafalias, 1997; Dafalias & Manzari, 2004; Taiebat & Dafalias, 2008).

A key strength of SANISAND lies in its ability to model critical state behaviour, where shear strain accumulation occurs at constant volume. The model defines a state parameter**,** introduced as $\psi = e - e_c$, by Been & Jefferies (1985), to represent the material's position relative to the critical state line. Both the bounding surface and phase transformation yield surfaces evolve based on the current effective volumetric stress and void ratio, ensuring consistency with critical state soil mechanics.

The SANISAND model is characterised by a narrow, wedge-shaped open yield surface in the triaxial *p-q* stress space, with its apex positioned at the origin. It illustrates the yield surface along with critical state, dilatancy, and bounding lines. The geometry demonstrates that the changes in stress ratio (q/p) predominantly control the relative sliding and rotational movement of sand particles. These microscopic interactions translate into macroscopic plastic shear and volumetric strains, enabling the model to reliably capture sand behaviour under a wide range of loading scenarios. Dafalias & Manzari (2004) defined a conical yield surface that generalises the wedge-shaped formulation from triaxial *p-q* space into three-dimensional space (Figure 1). This cone-shaped geometry enables the model to effectively capture important features of sand behaviour, such as cyclic loading, load reversals, and non-triaxial stress paths, due to its tensor-based representation of fabric evolution. The model is effective in simulating sandy soils across a wide range of relative densities and confining pressures using a unified set of material parameters (Arduino & Ghofrani, 2019). A comprehensive description of the SANISAND model can be found in Dafalias & Manzari (2004), while foundational concepts and earlier formulations are presented in Manzari & Dafalias (1997).

In geotechnical simulations involving large deformations, such as column penetration, the accuracy of the analysis not only depends on the numerical framework but also on the choice of the constitutive model. While the ALE method efficiently handles mesh quality and kinematic accuracy, a robust constitutive model is required to capture the true stress-strain behaviour of the soil. In this study, the SANISAND model is employed within the ALE framework to realistically represent the mechanical behaviour of sandy soils under complex loading conditions. The constitutive model for sandy soil has been integrated into the finite element software ABAQUS/Explicit through a user-defined material subroutine. Although ABAQUS includes an extensive library of material models and element types, advanced models are not available by default. In such cases, the user should develop their material models using user subroutines. In ABAQUS/Explicit, the user-defined material model is implemented using the subroutine VUMAT written in the FORTRAN language. During the analysis, the user subroutine is called at each integration point. Hence, it needs to be computationally efficient, robust and accurate. In this study, SANISAND was incorporated based on the VUMAT developed by Staubach et al. (2021), which includes 16 model parameters. Parameters can be calibrated using laboratory test data through the trial and error procedures.

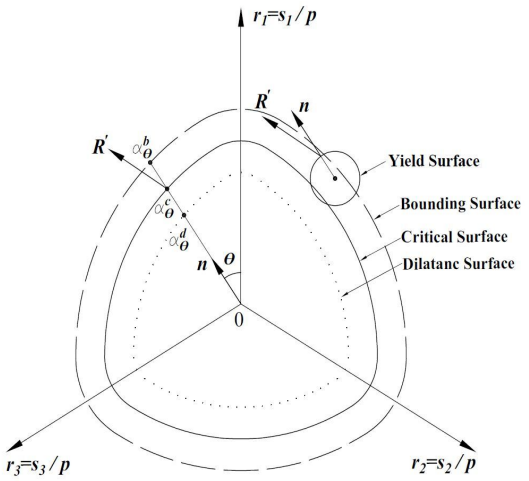

Figure 1. Schematic representation of the yield, critical, dilatancy, and bounding surfaces on the stress ratio π plane (Dafalias & Manzari (2004)).

3.1 *Parameter Calibration*

The SANISAND model parameters were calibrated by simulating the Consolidated Drained (CD) triaxial tests using ABAQUS/Explicit. The simulation was conducted using Ottawa F65 sand (Ramirez et al., 2018) with an initial void ratio of 0.7 under confining pressures (*Pc*) of 100 kPa, 200 kPa and 300 kPa. The calibrated parameters are listed in Table 1, which were extracted following the procedures outlined by Dafalias & Manzari (2004) and Taiebat & Dafalias (2008).

The model parameters e_0, λc, and ξ were determined by fitting the best-fit curve to the results of triaxial tests corresponding to the critical state in the e-p/p_{at} space. The parameter Mc was determined by plotting mean stress-deviatoric stress (p-q) from triaxial compression test data, which is the gradient of the line corresponding to the critical state. The parameter M_e was calculated following the same procedure applied for M_c, but based on triaxial tension test data. The ratio c is defined as $c = M_e/M_c$. For this analysis, a value of c = 0.735 was used based on prior research (Ramirez et al., 2018). The yield surface's shape, which is represented by a cone-shaped formulation, is governed by the parameter m. To achieve an adequate small-strain response, m was set to 0.02, in line with recommendations by Dafalias & Manzari (2004). The constant G_0 for sand was determined by adjusting the initial loading response of the deviatoric stress-strain (q-ε_q) from drained triaxial tests, considering the Equation given by Taiebat & Dafalias (2008). A Poisson's ratio (ν) of 0.05 was selected based on the literature (Ramirez et al., 2018; Kowalczyk, 2020). The hardening parameters, h_0 and c_h, were fine-tuned using an iterative trial and error method until the numerical results aligned closely with the experimental data. The values of n_b and n_d were established by following the procedure outlined by Taiebat & Dafalias (2008), which entails aligning the deviatoric stress-axial strain and volumetric strain-axial strain responses derived from drained monotonic triaxial tests. Figure 2 illustrates the comparison between the simulation outcomes and experimental data, displaying the relationship between deviatoric stress and axial strain. The simulations align well with the experimental findings (Ramirez et al., 2018), which confirms the validity of the calibrated SANISAND model parameters.

Table 1. SANISAND parameters.

Constant	Variable	Value
Atmospheric pressure (kPa)	p_a	100
Elasticity	G_0	125
	ν	0.05
Critical state	M_c	1.26
	c	0.735
	λ	0.0287
	e_0	0.78
	ξ	0.7
Yield surface	m	0.02
Plastic modulus constant	h_0	5
	c_h	0.968
	n_b	2.3
Dilatancy constant	A_0	0.626
	n_d	2.5
Fabric-dilatancy tensor	z_{max}	11
	c_z	500

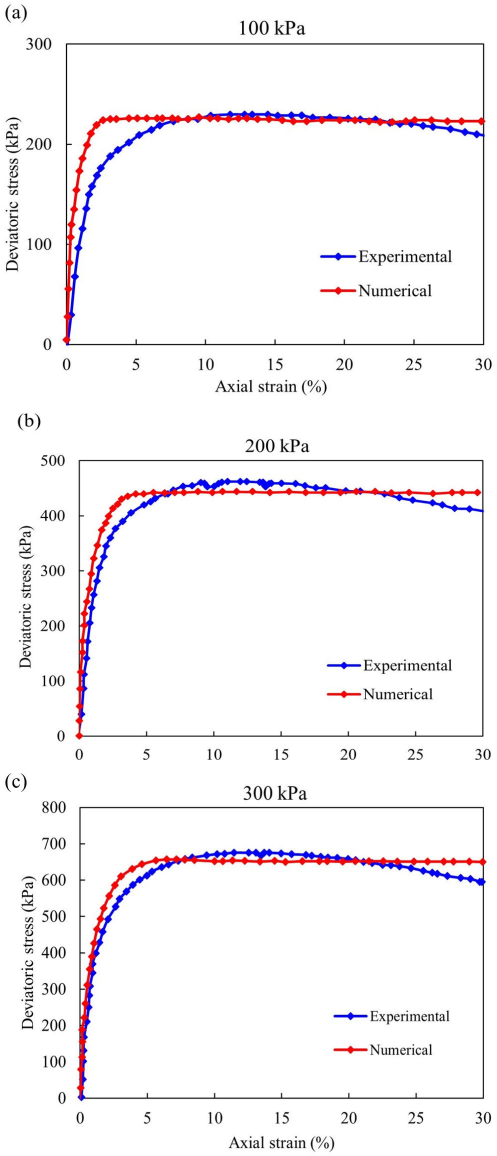

Figure 2. Numerical simulation and experimental results of drained triaxial tests under different confining pressures:(a) 100 kPa, (b) 200 kPa, and (c) 300 kPa.

4 NUMERICAL MODEL

In this study, an axisymmetric finite element model was created utilising the approach outlined by Henke & Grabe (2006), as illustrated in Figure 3, to simulate the installation of the column. For this study, a column with a diameter of 0.4 m was selected, which is within the typical range of auger sizes used in practice (250-500 mm), as reported by Menard (2025). A tube of 1 mm radius was modelled as a frictionless analytical rigid surface in contact with both the column and the surrounding soil, following the approach of Henke & Grabe (2006). It was included to prevent artificial shear stresses and unrealistic deformations of soil near the axis of symmetry, ensuring axisymmetric deformation during installation. As the column penetrates into the soil, it slides over the tube, separating the soil from the axis and generating realistic column-soil contact. The tube's small 1 mm radius minimised its influence on the overall soil response while maintaining numerical stability near the centreline. The model shown in Figure 4 extends 25D in both horizontal and vertical directions, where D is the diameter of the column. The column was

penetrated to a depth of approximately 5 m, which is approximately equivalent to 12.5*D*. Figure 4 depicts the finite element mesh used to simulate the column penetration with finer elements towards the column and coarser elements towards the boundary.

The bottom and right boundaries of the soil domain were restricted in both vertical and horizontal directions, while the left boundary was restrained horizontally. Element CAX4R, which is a four-node axisymmetric quadratic, reduced integration element, was used to model the soil domain. Analytical rigid surfaces were adopted to model both the column and the tube. The tube remained constrained in all directions throughout the analysis, whereas the column was only restrained laterally during its installation. Each rigid surface has a single reference point to which loads and the relevant boundary conditions were applied. The column-soil interaction was modelled using the contact algorithm, where a frictional interface is applied in this case. The rigid column is identified as the primary surface, while the soil surface in contact with the column is referred to as the secondary surface. The soil-column interaction was modelled using a surface-to-surface contact algorithm with a penalty approach. A constant friction coefficient of 0.4 was assigned to represent interface behaviour during installation. Although interface friction can vary with stress and density, a constant value was used as a practical simplification, since the primary increase in shaft resistance arises from the rise in radial stress captured by the model. The soil behaviour was captured using the SANISAND model, with parameters given in Table 1.

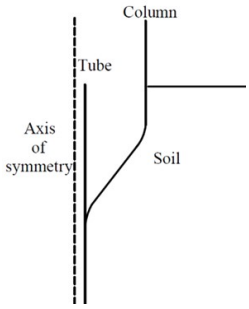

Figure 3. Configuration of the column and tube embedded in soil.

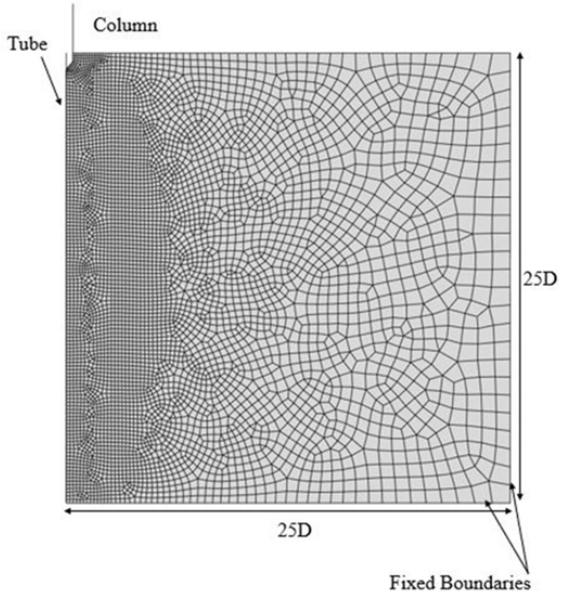

Figure 4. Axisymmetric finite element model used for column installation.

5 RESULTS

5.1 *Load-Displacement response*

A displacement-controlled boundary was used to simulate the penetration of the column. The vertical reaction produced during the penetration is shown in Figure 5 with the dimensionless penetration depth, *V*/*D,* where *V* is the vertical column penetration and *D* is the column diameter. The reaction force illustrates how the column's load-carrying capacity develops with the progression of column penetration.

At shallow penetration depths (*V*/*D* ≈ 1 to 3), the column penetration shows a relatively stiff response, requiring up to 1000 kN to penetrate to a depth of *D*. As the column advances further, resistance increases steadily with penetration, reaching approximately 3000 kN at *V*/*D* ≈ 7, and increasing up to 4100 kN at the final recorded penetration depth of *V*/*D* ≈ 12.5. This indicates that initially, as the column begins to penetrate, the load-carrying capacity appears to be relatively moderate. However, as the penetration progresses, the reaction force significantly escalates. This trend highlights the increasing resistance encountered by the column as it displaces soil and compacts the surrounding material.

To compare with conventional design methods, the bearing capacity of the column was also estimated using Equation (1) adopted from Plomteux et al. (2004), who applied an empirical relationship originally proposed by Sanglerat (1972) to pile design. In this Equation, coefficients k and k_1 are unitless empirical coefficients with k = 0.5, k_1 = 0.9 (usually $0.5<k_1<0.9$), A = cross-section of the CMC, q_c = cone tip resistance, Z = anchorage length, D = diameter of the CMC and *FOS* = factor of safety (Plomteux et al., 2004).

$$Q_u = \frac{(kAq_c + k_1 \frac{kq_c}{10} Z\pi D)}{FOS} \quad (1)$$

This Equation is based on the cone penetration resistance measured in the field. Hence, the cone tip resistance (q_c) was obtained from the relationship between q_c and effective vertical stress σ_{vo} for Ottawa F65 sand at different relative densities reported by Moug et al. (2019). The curve corresponding to a relative density of 40% was used in this study, yielding a calculated q_c value of 7302.6 kPa. Using the Equation, the calculated column capacity is approximately 2524 kN with a factor of safety of 1. In contrast, the numerical simulation predicted a capacity of up to 4100 kN, nearly 1.6 times higher. This significant difference highlights the expected variation between empirical design equations and detailed numerical simulations. Further validation would be needed to assess how closely each approach represents field behaviour.

These findings underline the importance of incorporating advanced numerical modelling techniques in the design of CMC. By utilising these modern methods, engineers can achieve a more accurate assessment of bearing capacities, ultimately leading to safer and more resilient foundation designs tailored to specific site conditions. This approach not only enhances structural integrity but also optimises material use, making it a more sustainable choice in construction practices. In particular, the simulation captures the mechanical effects of radial displacement and void ratio reduction, which are typically overlooked in design methods adopted in practice. Such installation-induced changes significantly improve the interaction between the column and the surrounding soil, resulting in greater load transfer efficiency. Consequently, relying solely on traditional equations could lead to overly conservative designs, while the use of calibrated numerical models enables a more realistic estimation of field performance.

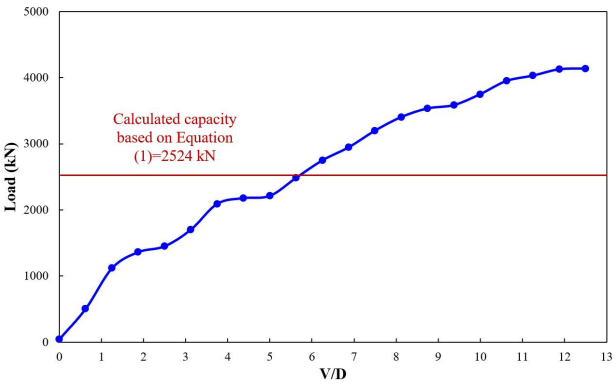

Figure 5. Load-Displacement response during column penetration.

5.2 *Identification of the disturbed zone*

The identification of the disturbed zone was based on evaluating the variation in radial stress, radial displacement, and void ratio around the column at a penetration depth of 12.5*D*, as illustrated in Figure 6. Radial stress (σ_r) distribution in Figure 6(a) reveals a concentrated high-stress region surrounding the column shaft and an additional stress concentration near the tip, which arises from the confinement and downward soil displacement that develops at the advancing column tip despite the predominantly radial movement of the surrounding soil. The stress values reach up to 6000 kPa, with a rapid decrease observed beyond a radial distance of approximately 1.5*D* from the edge of the column shaft. Outside this high-stress band (as indicated by the light blue zone with about 1000 kPa), the stress levels stabilise around 1000 kPa, which is about 17% of the peak mobilised radial stress. This indicates an area of confined soil and resistance mobilisation. Beyond approximately 1.5*D*, the radial stress reduces to around 1000 kPa and exhibits a stabilised pattern with no further significant variation. In this study, the disturbed zone was defined as the region where the mobilised radial stress remained substantially higher than the initial in-situ radial stress of approximately 38 kPa, representing an increase of about 26 times before reaching this stabilised level. Based on this combined criterion of elevated stress and subsequent stabilisation, the radial extent of the disturbed zone was identified as approximately 1.5*D*. This highlights how stress accumulates with penetration depth, reflecting the enhanced soil resistance and increased interaction between the column and the surrounding soil, which ultimately enhances the column's bearing capacity.

The radial displacement contours shown in Figure 6(b) effectively describe the mechanically disturbed zone, further confirming the radial extent of the zone. The maximum radial displacement occurs along the shaft, reaching approximately 0.15 m. Displacements above 0.05 m are confined within a radial distance of 1.5*D*. Beyond this region, radial displacements decrease around the column. Additionally, the blue regions near the column tip indicate negative radial soil movements toward the column, which is a result of downward soil movement at the tip during installation.

Void ratio variation, shown in Figure 6(c), was obtained directly from the SANISAND constitutive model, in which void ratio is defined as an internal state variable and is provided as a state variable output within the ABAQUS analysis. It reveals a low void ratio zone (light green to yellow regions), with values less than 0.63 surrounding the column. This represents approximately a 10% reduction from the initial void ratio of around 0.7, indicating soil densification near the shaft. The extent of this reduction defines an influence zone of approximately *D*, which is less than the disturbed zone identified from radial stress and displacement distributions. Unlike the more clearly depicted patterns seen in the radial stress and radial displacement contours, the disturbed zone boundary in the void ratio distribution is less distinct. This is largely due to the relatively small magnitude of void ratio changes and their narrow numerical range, making subtle gradients more challenging to capture. Beyond 1.5*D*, void ratio values generally exceed 0.67 and remain relatively stable, indicating that the effects of installation diminish rapidly with distance. Although the void ratio plot does confirm localised densification, it does not highlight the disturbed zone as clearly as the other two measures. Nevertheless, the observed densification suggests that the installation process effectively alters the soil behaviour, resulting in varying degrees of densification within a constrained area surrounding the column.

Based on these findings, the disturbed zone can be identified as extending up to approximately 1.5*D*. Within this zone, the soil experiences increased stresses and densification. This integrated interpretation supports a reliable identification of the installation-affected region, which is critical for understanding load transfer mechanisms, refining design models, and enhancing the prediction of CMC performance in sandy soils.

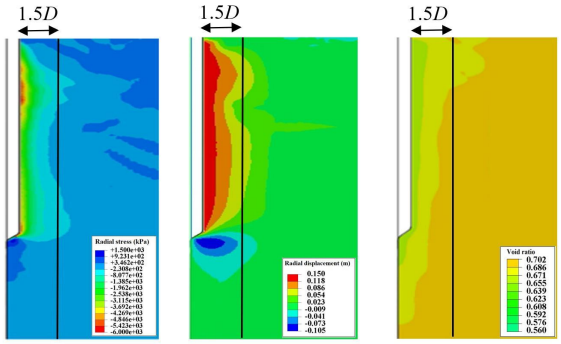

Figure 6. Variation of (a) Radial stress, (b) Radial displacement and (c) Void ratio at 12.5*D* depth.

6 CONCLUSIONS

This study presented a detailed numerical investigation of CMC penetration using the Arbitrary Lagrangian-Eulerian (ALE) approach implemented in ABAQUS/Explicit, combined with the SANISAND constitutive model to realistically capture the mechanical behaviour of sandy soils under large soil deformations. The analysis focused on four critical aspects: load-displacement response, stress distribution, void ratio and displacement evolution during column installation.

Radial stress distributions revealed the development of a high-stress region surrounding the column, particularly near the shaft and tip and stabilised beyond approximately 1.5*D* from the column shaft. This stress accumulation indicated the extent of soil confinement and interaction with the advancing column. Radial displacement patterns further confirmed this, with significant lateral movement observed within 1.5*D* from the shaft, gradually decreasing away from the column shaft. Understanding this behaviour is essential for optimising installation techniques and enhancing the reliability of performance predictions for Controlled Modulus Columns (CMC) in granular soils. Void ratio variation also provided an insight into the disturbed zone. The disturbed zone, based on void ratio changes, is confined to a very narrow region close to the column compared to that identified based on radial stress and displacement distributions.

These observations confirm that soil structure evolves markedly with depth and stress history, which has important implications for post-installation settlement, stiffness, and bearing capacity. Based on the results from all three indicators, stress, void ratio, and displacement, it can be concluded that the disturbed zone extends radially from the column surface up to approximately 1.5*D*. This zone represents the region where the soil is significantly influenced by installation, contributing to increased load transfer efficiency.

Overall, these results highlight the critical role of advanced numerical techniques in capturing the highly nonlinear, stress-path-dependent, and fabric-sensitive behaviour of cohesionless soils during CMC installation. The integration of the ALE method with the SANISAND model offers a powerful tool for researchers and practitioners to better predict column behaviour, optimise installation methods, and design more reliable ground improvement systems. These insights contribute to improving the safety, performance, and cost-effectiveness of geotechnical engineering solutions, particularly for applications involving deep penetration problems.

7 REFERENCES

Alamgir, M., Miura, N., Poorooshasb, H. & Madhav, M. 1996. Deformation analysis of soft ground reinforced by columnar inclusions. *Computers and Geotechnics,* 18**,** 267-290.

Arduino, P. & Ghofrani, A. 2019. Modelling liquefaction effects—from lateral spreading to soil-structure interaction. *Earthquake Geotechnical Engineering for Protection and Development of Environment and Constructions.* CRC Press.

Bakroon, M., Daryaei, R., Aubram, D. & Rackwitz, F. 2017. Arbitrary lagrangian-eulerian finite element formulations applied to geotechnical problems. *Numerical methods in geotechnics,* 41**,** 33-44.

Been, K. & Jefferies, M. G. 1985. A state parameter for sands. *Géotechnique,* 35**,** 99-112.

Chu, J., Varaksin, S., Klotz, U. & Menge, P. State of the art report: construction processes. 17th International Conference on Soil Mechanics & Geotechnical Engineering: TC17 meeting ground improvement, 2009.

Dafalias, Y. F. & Manzari, M. T. 2004. Simple plasticity sand model accounting for fabric change effects. *Journal of Engineering mechanics,* 130**,** 622-634.

Dassault-Système. 2025. *About ALE Adaptive Meshing* [Online]. Available: https://help.3ds.com/2025/english/dssimulia_established/SIMACAEANLRefMap/simaanl-c-aleover.htm?contextscope=all&id=95a68ce4209a4bc5905c068ce031838b [Accessed 11/08/2025].

Ekanayake, S. D., Liyanapathirana, D. & Leo, C. J. 2013. Influence zone around a closed-ended pile during vibratory driving. *Soil Dynamics and Earthquake Engineering,* 53**,** 26-36.

Han, J. 2015. *Principles and practice of ground improvement*, John Wiley & Sons.

Hannachi, N., Khalfallah, A., Leitão, C. & Rodrigues, D. M. Comparison between ALE and CEL finite element formulations to simulate friction stir spot welding. International Conference on Advanced Materials Mechanics & Manufacturing, 2021. Springer, 277-284.

Henke, S. & Grabe, J. Simulation of pile driving by 3-dimensional Finite-Element analysis. Proceedings of 17th European Young Geotechnical Engineers' Conference, 2006 Zagreb, Croatia. Croatian Geotechnical Society, 215-233.

Hu, Y. & Randolph, M. F. 1998. A practical numerical approach for large deformation problems in soil. *International Journal for Numerical and Analytical Methods in Geomechanics,* 22**,** 327-350.

Konkol, J. & Bałachowski, L. 2016. Large deformation finite element analysis of undrained pile installation. *Studia Geotechnica et Mechanica,* 38.

Kowalczyk, P. J. 2020. *Validation and application of advanced soil constitutive models in numerical modelling of soil and soil-structure interaction under seismic loading.* PhD PhD Thesis, University of Trento.

Larisch, M. D., Kelly, R. & Muttuvel, T. 2015. Improvement of Soft Soil Formations by Drilled Displacement Columns. *Ground Improvement Case Histories.*

Liyanapathirana, D. 2009. Arbitrary Lagrangian Eulerian based finite element analysis of cone penetration in soft clay. *Computers and Geotechnics,* 36**,** 851-860.

Liyanapathirana, D., Deeks, A. & Randolph, M. 2000. Numerical modelling of large deformations associated with driving of open-ended piles. *International Journal for Numerical and Analytical Methods in Geomechanics,* 24**,** 1079-1101.

Liyanapathirana, D. S. & Ekanayake, S. D. 2016. Application of EPS geofoam in attenuating ground vibrations during vibratory pile driving. *Geotextiles and Geomembranes,* 44**,** 59-69.

Manzari, M. T. & Dafalias, Y. F. 1997. A critical state two-surface plasticity model for sands. *Géotechnique,* 47**,** 255-272.

Massé, F., Carey, M. J. & Ingram, I. Controlled Modulus Columns (CMC) : Application to the support of Mechanically Stabilized Earth Walls (MSE Walls). Pan-Am CGS Geotechnical Conference, 2011 Toronto, Ontario, Canada.

Menard. 2025. *Controlled Modulus Columns (CMC)* [Online]. Available: https://www.menard-group.com/soil-expert-portfolio/controlled-modulus-columns/ [Accessed 02/02/2023].

Moug, D., Price, A., Darby, K., Bastidas, A. P., Boulanger, R. & Dejong, J. 2019. Mechanistic development of CPT-based cyclic strength relationships for Ottawa sand. *Earthquake Geotechnical Engineering for Protection and Development of Environment and Constructions.* CRC Press.

Plomteux, C., Porbaha, A. & Spaulding, C. 2004. CMC foundation system for embankment support-A case history. *GeoSupport 2004: Drilled Shafts, Micropiling, Deep Mixing, Remedial Methods, and Specialty Foundation Systems.* Orlando Florida, United States.

Ramirez, J., Barrero, A. R., Chen, L., Dashti, S., Ghofrani, A., Taiebat, M. & Arduino, P. 2018. Site response in a layered liquefiable deposit: evaluation of different numerical tools and methodologies with centrifuge experimental results. *Journal of Geotechnical and Geoenvironmental Engineering,* 144**,** 04018073.

Sanglerat, G. 1972. *The penetrometer and soil exploration: Interpretation of penetration diagrams - theory and practice*.

Staubach, P., Machaček, J. & Wichtmann, T. 2021. Large-deformation analysis of pile installation with subsequent lateral loading: Sanisand vs. Hypoplasticity. *Soil Dynamics and Earthquake Engineering,* 151**,** 106964.

Suleiman, M. T., Ni, L., Davis, C., Lin, H. & Xiao, S. 2016. Installation Effects of Controlled Modulus Column Ground Improvement Piles on Surrounding Soil. *Journal of Geotechnical and Geoenvironmental Engineering,* 142.

Taiebat, M. & Dafalias, Y. F. 2008. SANISAND: Simple anisotropic sand plasticity model. *International Journal for Numerical and Analytical Methods in Geomechanics,* 32**,** 915-948.

Varaksin, S., Hamidi, B. & Racinais, J. 2014. The Thin Line between Deep Foundations and Soil Improvement. *Journal of Perm Polytechnic University and National Research - Construction and Architecture* 3, 9-32.

Wang, D., Bienen, B., Nazem, M., Tian, Y., Zheng, J., Pucker, T. & Randolph, M. F. 2015. Large deformation finite element analyses in geotechnical engineering. *Computers and Geotechnics,* 65**,** 104-114.

Wotzlaw, M., Daryaei, R., Aubram, D. & Rackwitz, F. 2024. Ghost material in geotechnical applications of the CEL method. *Computers and Geotechnics,* 167**,** 106082.

Yang, Z. X., Gao, Y. Y., Jardine, R. J., Guo, W. B. & Wang, D. 2020. Large Deformation Finite-Element Simulation of Displacement-Pile Installation Experiments in Sand. *Journal of Geotechnical and Geoenvironmental Engineering,* 146**,** 04020044.